

1           **STRESS-BLOCK PARAMETERS FOR REINFORCED CONCRETE**  
2                                   **BEAMS DURING FIRE EVENTS**

3                                   S.F. El-Fitiany and M.A. Youssef\*

4                   Department of Civil and Environmental Engineering, The University of Western Ontario,  
5                                   London, ON, Canada N6A 5B9  
6

7   **Biography:**

8   ACI student member **S.F. El-Fitiany** is a Ph.D. candidate at The University of Western Ontario,  
9   Canada. Mr. El-Fitiany obtained his M.E.Sc. from The University of Western Ontario and his  
10   B.Sc. from Alexandria University, Egypt. His research interests include behavior of structures  
11   during and after exposure to fire and development of performance based fire design approaches.

12   ACI member **M.A. Youssef** is an associate professor of Civil Engineering at The University of  
13   Western Ontario. Dr. Youssef received his Ph.D. from McMaster University, Hamilton, Ontario.  
14   His research interests include: modeling of reinforced concrete structures, fire resilience of  
15   concrete structures, use of innovative materials (Fiber Reinforced Polymers, FRP, and Shape  
16   Memory Alloys, SMA) to upgrade the capacity of existing structures, using SMA to minimize  
17   structural damage during earthquakes, and seismic capacity of existing structures.

---

\* Corresponding authors: E-mail: [youssef@uwo.ca](mailto:youssef@uwo.ca), Phone: 519-661-2111 Ext. 88661

## ABSTRACT

1  
2 Fire safety is a critical criterion for designing reinforced concrete (RC) structures. New codes are  
3 moving towards Performance-based design. Conducting full scale experiments and  
4 comprehensive finite element simulations are usually expensive and time consuming options for  
5 designers to achieve specific fire performance. A simplified sectional analysis methodology that  
6 tracks the axial and flexural behavior of RC square sections subjected to elevated temperatures  
7 from their four sides was previously developed and validated by the authors. In the first part of  
8 this paper, the proposed methodology is extended to cover rectangular beams subjected to  
9 standard ASTM-E119 fire from three sides. An extensive parametric study is then conducted to  
10 study the distribution of the concrete compression stresses at different ASTM-E119 fire  
11 durations. Based on the parametric study, simple equations expressing the equivalent stress-block  
12 parameters at elevated temperatures are presented. These equations can be utilized by designers  
13 to accurately estimate the flexure capacity of simply supported and continuous beams exposed to  
14 fire temperature.

15  
16 **Keywords:** Concrete; Elevated temperatures; Sectional analysis; Fire resistance, Stress-block  
17 parameters.

## INTRODUCTION

18  
19  
20 Concrete as well as steel reinforcing bars experience significant deterioration when subjected to  
21 elevated temperatures<sup>1</sup>. This deterioration is accompanied by the generation of thermal and  
22 transient strains which adds to the complexity of estimating the flexural capacity of a reinforced  
23 concrete (RC) section at elevated temperatures. Currently, concrete structures are designed for  
24 fire safety using prescribed methods that are based on computational modeling and experimental

1 investigations. These methods usually specify the minimum cross-section dimensions and clear  
2 cover to achieve specific fire ratings. As new codes are moving towards performance-based  
3 design and conducting experimental tests to satisfy different fire scenarios would be an expensive  
4 solution, numerous design tools are needed by design engineers<sup>2</sup>. One of these tools would  
5 facilitate the estimation of the flexural behavior of a RC beam at elevated temperatures.

6 A simplified method to track the axial and/or the flexural behavior of square column sections  
7 subjected to fire at their four sides was previously introduced by El-Fitiany and Youssef<sup>3</sup>. This  
8 paper starts by extending the proposed method to be applicable to RC beams exposed to fire from  
9 three sides. The overall behavior of RC beams during fire exposure is tracked by constructing the  
10 moment-curvature relationships at different fire durations. The unrestrained simply supported  
11 beam tested by Lin et al.<sup>4</sup>, Fig. 1a, is taken as an illustrative example for the proposed  
12 methodology. The tested beam has a normal strength concrete with carbonate aggregate and  
13 subjected to ASTM-E119 standard fire.

14 Civil engineers are familiar with using the concrete stress-block parameters in calculating the  
15 ultimate capacity of RC members at ambient temperature. These parameters convert the parabolic  
16 distribution of concrete compression stresses to an idealized rectangular stress-block. Evaluation  
17 of those parameters at elevated temperatures allows designers to easily estimate the flexural  
18 capacity of RC beams during fire exposure. The second part of this paper presents a parametric  
19 study to evaluate the compressive stresses distribution for different rectangular concrete cross-  
20 sections. The effect of different parameters including section dimensions, reinforcement ratio,  
21 concrete strength, fire duration, and aggregate type is evaluated.

22

23

24

## RESEARCH SIGNIFICANCE

1  
2 The proposed simplified method extends the use of sectional analysis to be applicable at elevated  
3 temperatures. Designers are familiar with this method at ambient temperature, which will allow  
4 them to use it in their fire calculations. The ultimate/nominal flexural capacity of RC beams can  
5 be evaluated at ambient temperature using equivalent stress-block parameters. No specific study  
6 was conducted addressing the effect of fire temperature on such parameters. The second part of  
7 this paper presents an extensive parametric study on the non-linear distribution of compression  
8 stresses for a number of rectangular cross-sections at different ASTM-E119 fire durations up to  
9 2.5 hr. It ends by providing simplified equations for designers to allow them to estimate the  
10 stress-block parameters at elevated temperatures.

## SECTIONAL ANALYSIS AT AMBIENT TEMPERATURE

11  
12  
13 At ambient temperature, RC sections are analyzed using the well-known sectional analysis  
14 approach<sup>5</sup>. For cases of single curvature, i.e. bending about horizontal axis, the concrete section is  
15 divided into horizontal discrete fibers. Utilizing the uniaxial stress-strain relationship for each  
16 fiber and taking into account equilibrium and kinematics, the mechanical behavior of the section  
17 is analyzed. To simplify the analysis, two variables can be assumed; incremental centroidal axial  
18 strain,  $\Delta\varepsilon_c$ , and incremental curvature,  $\Delta\psi$ . Assuming a linear strain distribution, the incremental  
19 moment and axial force are obtained using Eq. (1).

$$20 \begin{pmatrix} \Delta M \\ \Delta P \end{pmatrix} = \begin{pmatrix} \sum_{i=1}^n E_i \times A_i \times y_i^2 & -\sum_{i=1}^n E_i \times A_i \times y_i \\ -\sum_{i=1}^n E_i \times A_i \times y_i & \sum_{i=1}^n E_i \times A_i \end{pmatrix} \times \begin{pmatrix} \Delta\psi \\ \Delta\varepsilon_c \end{pmatrix} \quad (1)$$

1 Where  $E_i$  is the modulus of elasticity of layer  $i$ ,  $A_i$  is the area of layer  $i$ ,  $y_i$  is the distance between  
2 the center of area of layer  $i$  and center of area of the cross-section.

3 For a given axial load, the moment-curvature behavior is obtained in two stages. In the first stage,  
4 the axial strain is increased incrementally while curvature is kept equal to zero until reaching the  
5 required axial load. In the second stage, the axial load is kept constant and the applied curvature  
6 is increased. The corresponding change in the axial strain and the moment are calculated using  
7 Eq. (1). This process is repeated until reaching the required curvature value.

8

## 9 SECTIONAL ANALYSIS AT ELEVATED TEMPERATURES

10 To apply sectional analysis at elevated temperatures, a number of modifications were proposed  
11 and validated by El-Fitiany and Youssef<sup>3</sup>. These modifications account for the two dimensional  
12 temperature gradient within the concrete cross section, which affects its homogeneity and  
13 increase the nonlinearity of the mechanical strain distribution. The following sections generalize  
14 the previously developed method to be applicable to rectangular sections exposed to fire  
15 temperature at a number of their sides. Beam B1, shown in Fig. 1, is used to illustrate the  
16 concepts. The beam is exposed to ASTM-E119 fire at three of its faces for duration of an hour.

17

### 18 Concrete and steel constitutive models

19 The constitutive models proposed by Youssef and Mofteh<sup>6</sup> are adopted and their application to  
20 beam B1 is presented in the following sub-sections.

21

### 22 Concrete compressive strength

23 Hertz model<sup>7</sup>, Eq. (2), is used to predict the reduced concrete compressive strength ( $f'_{cT}$ ) at  
24 elevated temperatures. If concrete is loaded prior to fire,  $f'_{cT}$  should be increased by 25%<sup>7</sup>.

1  $f'_{cT} = R \times f'_c$  (2.a)

2  $R = \frac{1}{1 + \frac{T}{15,000} + \left(\frac{T}{800}\right)^2 + \left(\frac{T}{570}\right)^8 + \left(\frac{T}{100,000}\right)^{64}}$  , for concrete with siliceous aggregate (2.b)

3  $R = \frac{1}{1 + \frac{T}{100,000} + \left(\frac{T}{1080}\right)^2 + \left(\frac{T}{690}\right)^8 + \left(\frac{T}{1000}\right)^{64}}$  , for concrete with carbonate aggregate (2.c)

4  
 5 Where  $R$  is a reduction factor,  $T$  is the temperature in degree Celsius [ $1\text{ }^\circ\text{F} = 1.8\text{ }^\circ\text{C} + 32$ ], and  $f'_c$   
 6 is the concrete compressive strength at ambient temperature.

7

8 **Fire induced strains**

9 Total concrete strain at elevated temperatures ( $\varepsilon_{tot}$ ) is composed of three terms<sup>6</sup>: instantaneous  
 10 stress related strain ( $\varepsilon_{fT}$ ), unrestrained thermal strain ( $\varepsilon_{th}$ ), and transient creep strain ( $\varepsilon_{tr}$ ). The  
 11 value of  $\varepsilon_{fT}$  at the peak stress ( $\varepsilon_{oT}$ ) defines the stress-strain relationship during the heating stage  
 12 and can be predicted using the model proposed by Terro<sup>8</sup>, Eq. (3). Flexural RC elements have a  
 13 variant stress values within concrete compression zone which implies different preloading  
 14 levels  $\lambda_L$  for each fiber.

15  $\varepsilon_{oT} = (50\lambda_L^2 - 15\lambda_L + 1) \varepsilon_{o1} + 20(\lambda_L - 5\lambda_L^2) \varepsilon_{o2} + 5(10\lambda_L^2 - \lambda_L) \times 0.002$  (3)

16 where  $\varepsilon_{o1} = 2.05 \times 10^{-3} + 3.08 \times 10^{-6} T + 6.17 \times 10^{-9} T^2 + 6.58 \times 10^{-12} T^3$   
 $\varepsilon_{o2} = 2.03 \times 10^{-3} + 1.27 \times 10^{-6} T + 2.17 \times 10^{-9} T^2 + 1.64 \times 10^{-12} T^3$

17  $\varepsilon_{th}$  is the free thermal strain resulting from fire temperature and can be predicted using the  
 18 Eurocode model<sup>6</sup>, Eq. (4).

1  $\varepsilon_{th} = -1.8 \times 10^{-4} + 9 \times 10^{-6} (T - 20) + 2.3 \times 10^{-11} (T - 20)^3 \leq 14 \times 10^{-3}$  , for concrete

2 with siliceous aggregate (4.a)

3  $\varepsilon_{th} = -1.2 \times 10^{-4} + 6 \times 10^{-6} (T - 20) + 1.4 \times 10^{-11} (T - 20)^3 \leq 12 \times 10^{-3}$  , for concrete

4 with carbonate aggregate (4.b)

5  $\varepsilon_{tr}$  is induced during the first heating cycle of loaded concrete and is considered the largest

6 component of the total strain. Its value can be estimated using Terro's model<sup>8</sup>.

$$\varepsilon_{tr} = \varepsilon_{0.3} \times \left( 0.032 + 3.226 \frac{f_c}{f'_c} \right) \frac{V_a}{0.65} \quad (5)$$

Where

7  $V_a$  is the volume fraction of aggregates

$\varepsilon_{0.3}$  is the transient creep strain for initial axial stress of  $0.3 f'_c$ , and is given by Eq. (6)

$$\varepsilon_{0.3} = 43.87 \times 10^{-6} - 2.73 \times 10^{-8} T - 6.35 \times 10^{-8} T^2 + 2.19 \times 10^{-10} T^3 - 2.77 \times 10^{-13} T^4 \quad (6)$$

8

## 9 Reinforcing steel tensile stress-strain relationship

10 Lie's model<sup>1</sup> is used to predict the reduced yield strength of reinforcing bars  $f_{yT}$ , Eq. (7).

$$f_{yT} = \left( 1 + \frac{T}{900 \times \ln(T/1750)} \right) \times f_y \quad 0 < T \leq 600 \text{ } ^\circ\text{C} \quad [32 < T \leq 1112 \text{ } ^\circ\text{F}] \quad (7.a)$$

$$f_{yT} = \left( \frac{340 - 0.34 \times T}{T - 240} \right) \times f_y \quad 600 < T \leq 1000 \text{ } ^\circ\text{C} \quad [32 < T \leq 1112 \text{ } ^\circ\text{F}] \quad (7.b)$$

13 Lie<sup>1</sup> has also proposed another model representing a general stress-strain ( $f_{sT} - \varepsilon_{sT}$ ) relationship

14 of reinforcing bars at elevated temperatures, Eq. (8). The effect of creep of steel bars is found to

15 have a minor effect on the behavior of RC sections during fire exposure<sup>9</sup> and, thus is not included

16 in this study.

$$f_{sT} = \frac{f(T, 0.001)}{0.001} \times \varepsilon_{sT} \quad \varepsilon_{sT} \leq \varepsilon_p \quad (8.a)$$

17

$$1 \quad f_{sT} = \frac{f(T,0.001)}{0.001} \times \varepsilon_p + f(T, [\varepsilon_{sT} - \varepsilon_p + 0.001]) - f(T,0.001) \quad \varepsilon_{sT} > \varepsilon_p \quad (8.b)$$

$$2 \quad \varepsilon_p = 4 \times 10^{-6} f_y \quad (8.c)$$

$$3 \quad f(T,0.001) = (50 - 0.04T) \times [1 - e^{(-30+0.03T)\sqrt{0.001}}] \times 6.9 \quad (8.d)$$

4

### 5 **Concrete compressive stress-strain relationship**

6 The model proposed by Youssef and Moftah<sup>6</sup> is adopted in this study. The model includes  
 7 simplified representation of transient creep strains. The relationship between the compressive  
 8 stress,  $f_{cT}$ , and the corresponding compressive strain,  $\varepsilon_{cT}$ , is given by Eq. (9).

$$9 \quad f_{cT} = K_{hT} \times f'_{cT} \left[ 2 \times \left( \frac{\varepsilon_{cT}}{\varepsilon_{oT} + \varepsilon_{tr}} \right) - \left( \frac{\varepsilon_{cT}}{\varepsilon_{oT} + \varepsilon_{tr}} \right)^2 \right] \quad \varepsilon_{cT} \leq \varepsilon_{oT} + \varepsilon_{tr} \quad (9.a)$$

$$10 \quad f_{cT} = K_{hT} \times f'_{cT} [1 - Z(\varepsilon_{cT} - \varepsilon_{oT} - \varepsilon_{tr})] \quad \geq 0.2 \times f'_{cT} \quad \varepsilon_{oT} \geq \varepsilon_{oT} \varepsilon_{tr} \quad (9.b)$$

11 where,

$$12 \quad K_{hT} \text{ (confinment factor)} = 1 + \frac{\rho_s \times f_{yT}}{f'_{cT}} \quad (9.c)$$

$$13 \quad \rho_s = \frac{\text{volume of transverse reinforcement}}{\text{volume of concrete core measured to their perimeter}}$$

14  $f_{yT}$  is the reduced yield strength for the stirrups at elevated temperature

15  $Z$  is the slope of the descending branch of the concrete stress-strain relationship and is given by

16 Eq. (9.d)

$$17 \quad Z = \frac{0.5}{\frac{3 + 0.29 f'_c}{145 f'_c - 1000} \times \frac{\varepsilon_{oT}}{\varepsilon_o} - \varepsilon_{oT}} \quad (9.d)$$

1 The ultimate compressive strain at failure is assumed to be 0.0035 in the ambient condition  
2 according to the Canadian standards CSA A23.3-04<sup>10</sup>. Due to the limited literature on the failure  
3 compressive strain at elevated temperature, this value is increased by the transient strain  $\varepsilon_{tr}$  as  
4 proposed by El-Fitiany and Youssef<sup>3</sup>.

$$5 \quad \varepsilon_{cuT} = \varepsilon_{cu} + \varepsilon_{tr} \quad (10)$$

6

### 7 **Heat transfer model**

8 Several methods were developed to predict the temperature distribution in a concrete section  
9 during fire exposure<sup>1</sup>. The Finite Difference Method (FDM) is chosen in this research because of  
10 its ability to account for irregular shapes, its accuracy, and the ease of implementation in any  
11 programming code. A detailed description of the FDM, in the form of prescribed equations, is  
12 given by Lie et al.<sup>1</sup>.

13 For beam B1, a 45 degree heat transfer mesh of 5.4 mm by 5.4 mm [0.21 in] square elements is  
14 generated as shown in Fig. 2. Based on the size of the elements, the total fire duration ( $\tau_f = 1$   
15 hour), is divided into time steps  $\Delta \tau_f$  of 4.2 seconds. Concrete initial moisture content is assumed  
16 to be zero due to its negligible effect on the temperature predictions<sup>1</sup>. A heat analysis based on  
17 the FDM is then conducted and the temperatures for steel bars were found to range from 302 °C  
18 [576 °F] to 513 °C [955 °F]. Fig. 3 shows a comparison between the average measured  
19 temperatures of bottom steel bars by Lin et al.<sup>4</sup> and the FDM predictions at different fire  
20 durations. To allow using sectional analysis, the 45 degree mesh elements are converted to  
21 horizontal square mesh elements<sup>1,3</sup>. The temperature at the center of each square element, Fig. 2b,  
22 is taken as the average temperature of the adjacent 45 degree mesh elements.

23

## 1 **Average layer temperature**

2 The methodology proposed by El-Fitiany and Youssef<sup>3</sup> is adopted. The square mesh elements are  
3 grouped into horizontal fibers to simplify the use of sectional analysis. Therefore, an equivalent  
4 temperature  $T_i$  has to be assigned for each fiber to allow estimating the concrete compressive  
5 strength, its modulus of elasticity, transient creep and thermal strains. To accurately predict the  
6 behavior using sectional analysis, El-Fitiany and Youssef<sup>3</sup> suggested the use of two different  $T_i$ 's,  
7 one for estimating stresses and the other for strain values. It is clear from Eq. (1) that the  
8 tangential modulus of elasticity is the most important factor, thus it is proposed to estimate the  
9 first average layer temperature such that it produces the average modulus of elasticity for the  
10 square elements within the layer. At elevated temperatures, initial modulus of elasticity of loaded  
11 concrete is proportional to its reduced compressive strength<sup>6</sup>. Therefore, the first average  
12 temperature distribution for each fiber is based on the average strength of the square mesh  
13 elements, Fig. 2d, composing this layer. The second average temperature distribution is used to  
14 estimate the thermal and transient creep strains. Eqs. (4) and (5) show that they are proportional  
15 to the fire temperature and, this second temperature is equal to the algebraic average of the square  
16 mesh elements composing this layer. Fig. 4 shows the two distributions for the analyzed beam B1  
17 after one hour of ASTM-E119 standard fire exposure. The temperature of steel bars can be  
18 assumed to be the same as the temperature of the square mesh element within which they are  
19 located<sup>1</sup>.

20

21

## 22 **Thermal and effective strain calculation**

23 Fig. 5 shows the expected linear distribution of total strains ( $\epsilon_{tot}$ ) under a pure bending moment  
24 (M). This linear shape is based on the fact that plane sections remain plane after loading, which is

1 still valid at elevated temperatures<sup>11,12</sup>. El-Fitiany and Youssef<sup>3</sup> used the same principle but their  
2 total strain was having a constant value representing the case for a section exposed to fire from  
3 four sides. The distribution of  $\varepsilon_{th}$  for a rectangular cross-section subjected to fire temperature  
4 from three sides is shown in Fig. 5.

5 For unrestrained concrete sections, the effective strain ( $\varepsilon_{eT}$ ) can be calculated by subtracting  
6 concrete and steel thermal strains from the total strain. The nonlinear distribution of thermal  
7 strains results in a nonlinear effective (mechanical) strain distribution, Fig. 5. As Eq. (1) is only  
8 applicable for linear strain distributions, the following sub-sections propose a methodology to  
9 conduct sectional analysis for the non-linear varying effective strain distribution.

10

### 11 **Isolation of thermal strain component for beam sections**

12 For square column sections exposed to fire temperature from four sides, details for thermal strain  
13 equilibrium are given by El-Fitiany and Youssef<sup>3</sup>. For the case of a rectangular cross-section  
14 exposed to fire from three sides, the thermal strain is expected to be asymmetric as shown in Fig.

15 5. The equivalent shape is defined by the mid-height axial strain ( $\overline{\varepsilon_{th}}$ ) and the curvature ( $\overline{\psi_{th}}$ ),

16 Figs. 5 and 6. The values of  $\overline{\varepsilon_{th}}$  and  $\overline{\psi_{th}}$  are evaluated such that the axial forces and bending  
17 moments in concrete and steel layers resulting from the difference between the actual thermal  
18 strain distribution and  $\overline{\varepsilon_{th}}$  are in self equilibrium. An iterative procedure is used to calculate the

19 values of  $\overline{\varepsilon_{th}}$  and  $\overline{\psi_{th}}$  such that the forces, shown in Fig. 6.b, are producing zero axial force and  
20 zero moment. Concrete tensile strength is neglected in the analysis.

21 Fig. 6.a shows the nonlinear thermal strain distribution for the studied beam B1 after 1 hr  
22 standard ASTM-E119 fire exposure. The presented thermal strain distribution is converted to a  
23 linear distribution by considering section equilibrium. The equivalent uniform strain reflects the

1 actual deformation of the concrete section under zero external loads and moments. Differences  
2 between the non-linear and equivalent uniform strains represent concrete and steel internal  
3 stresses that are in equilibrium.

4

#### 5 **Thermally induced stresses**

6 The conversion from the actual nonlinear strain distribution to the equivalent linear distribution  
7 induces self-equilibrating internal strains ( $\varepsilon_{\sigma th}$ ), Fig. 6.b. These internal strains are part of  
8 mechanical strains required to retain the geometric linearity of B1's cross-section. To account for  
9 these strains, they are included as initial strains for each concrete and/or steel fiber.

10

### 11 **ANALYSIS STEPS OF RC BEAMS UNDER FIRE LOADING**

12 It can be concluded from the previous sections that the sectional analysis can be divided into  
13 three main steps;

14 1. The heat transfer model is applied and the heat gradient through the cross section is predicted.

15 The average temperatures for each layer are then obtained.

16 2. The equivalent uniform thermal strain  $\overline{\varepsilon_{th}}$  and the curvature  $\overline{\psi_{th}}$  are then calculated by  
17 equilibrating the forces in the concrete and steel layers resulting from the actual thermal strain  
18 distribution. The difference between the actual and uniform strain distributions represents the  
19 induced strains  $\varepsilon_{\sigma th}$  in concrete and steel layers to satisfy the section geometry. These strains are  
20 considered as initial strains in the following step.

21 3. Sectional analysis is conducted to construct the moment-curvature diagrams.

22

23

## 1 **Validation of the sectional analysis methodology**

2 Moment-curvature curves represent the flexural behavior of a RC section under specified axial  
3 load level ( $\lambda = f_c / f'_c$ ). Fig. 7 shows the effect of 1 hr standard ASTM-E119 fire exposure on the  
4 studied unrestrained section of beam B1 ( $\lambda$  equals to zero). As shown in Fig. 7, elevated  
5 temperatures increase the ductility and reduce the capacity of RC sections during fire exposure.  
6 The initial point of the moment-curvature diagram after 1 hr fire exposure defines the equilibrium  
7 curvature  $\overline{\psi}_{th}$ . This curvature value represents the initial rotation of B1 due to the non-linear  
8 thermal distribution combined with the material weakening. This initial curvature will occur  
9 regardless of the external effect of the applied moments.

10 The moment-curvature diagrams were constructed for beam B1 at different fire durations. The  
11 vertical deflection  $w^*$  at each time step was estimated by applying the moment-area method to the  
12 estimated curvature distribution along the beam length. The obtained results are plotted in Fig. 8.  
13 An excellent matching is found between the sectional analysis, the FEM conducted by Kodur and  
14 Dwaikat<sup>2</sup>, and the experimental results (up to 80 minutes). Failure criteria proposed by BS 476  
15 and adopted by Kodur and Dwaikat<sup>2</sup> are used. These criteria are setting limits for the maximum  
16 allowable deflection, Eq. (11), and maximum rate of deflection, Eq. (12).

$$17 \Delta_{\max} = \frac{L}{20} = 305 \text{ mm [12 in]} \quad (11)$$

$$\left( \frac{\partial \Delta}{\partial t} \right)_{\max} = \frac{L^2}{9000d} = 13 \text{ mm/minute [0.51 in/minute]} \quad (12)$$

18 Where  $L$  is the span between the supports (mm) and  $d$  is the effective depth of the beam (mm) [1  
19 in = 25.4 mm]

20 As shown in Fig. 8, the proposed sectional analysis results in about 17 minutes difference in  
21 predicting failure compared with the reported fire test resistance.

1  
2  
3  
4  
5  
6  
7  
8  
9  
10  
11  
12  
13  
14  
15  
16  
17  
18  
19  
20  
21  
22

### STRESS-BLOCK PARAMETERS AT AMBIENT TEMPERATURE

Reinforced concrete beams are currently designed for flexure at ambient conditions by assuming a linear strain distribution and converting the nonlinear stress distribution to an equivalent stress-block. This conversion is done using the stress-block parameters  $\alpha_1$  and  $\beta_1$ . The recommended values for the stress-block parameters at ambient temperature in the Canadian code CSA A23.3-04<sup>10</sup> depend on  $f'_c$  to account for high strength concrete and are given by:

$$\alpha_1 = 0.85 - 0.0015 \times f'_c \tag{13.a}$$

$$\beta_1 = 0.97 - 0.0025 \times f'_c \tag{13.b}$$

The nominal moment at failure  $M_n$  can therefore be calculated from section equilibrium as follows

$$C = \alpha_1 \times f'_c \times \beta_1 \times c \times b \tag{14.a}$$

$$T_s = f_y \times A_s \tag{14.b}$$

$$C = T_s \quad (\text{calculate } c) \tag{14.c}$$

$$M_n = (C \text{ or } T_s) \times \left( d - \frac{\beta_1 \times c}{2} \right) \tag{14.d}$$

Where  $C$  is the compression force in the concrete,  $c$  is the depth of neutral axis,  $b$  is the width of the compression zone,  $T_s$  is the tension force in steel assuming yielding or reinforcement,  $f_y$  is the yield stress of steel bars,  $A_s$  is the area of tensile steel bars, and  $d$  is the effective depth of the section.

## STRESS-BLOCK PARAMETERS AT ELEVATED TEMPERATURES

The effect of fire temperature on the ambient stress-block parameters  $\alpha_1$  and  $\beta_1$  is evaluated in this section through an extensive parametric study. A total of 28 rectangular cross-sections are analyzed to study the stress distribution at different fire durations. Table 1 shows details of the beams that are subjected to sagging bending moments (positive moments). On the other hand, Table 2 shows details of beams that are subjected to hogging bending moments (negative moments). The studied parameters are; fire duration ( $\tau_f$ ), geometry of the sections ( $b$  and  $h$ ), reinforcement ratio ( $\rho$ ) and configuration, concrete compressive strength ( $f'_c$ ), and aggregate type. The effect of compression reinforcement is neglected for simplicity.

Fig. 9 shows details for the studied cross-sections. All the beams are subjected to the standard ASTM-E119 fire from three faces, i.e. the two sides and the bottom surface of each beam. A sectional analysis was conducted for each beam at different fire durations starting from 0.0 hr and up to 2.5 hr with a time interval of 15 min. For each time step, the stress-block parameters at elevated temperature  $\alpha_{1T}$  and  $\beta_{1T}$  are evaluated by predicting the total strain distribution ( $\epsilon_{tot}$ ) at failure using the proposed sectional analysis methodology. The mechanical strain ( $\epsilon_{cT}$ ) is then isolated and the stress distribution is obtained based on it. The following sub-sections explain these steps for beams B4, sagging moment, and B18, hogging moment.

### Behavior of beams subjected to sagging moments during fire

A heat transfer analysis was conducted for beam B4. The height of the beam was slightly increased to 705 mm [27.8 in] to retain the aspect ratio of the 45 degree heat transfer mesh. Fig. 10 shows the average temperature distributions along B4 cross-section height.

1 The studied beam B4 was analyzed using the proposed sectional analysis methodology. A  
2 constant spacing for stirrups of 600 mm [23.6 in] was assumed. Fig. 10 shows the predicted total  
3 linear strain distribution at failure. The mechanical strain  $\varepsilon_{cT}$  can be isolated from the total strain  
4  $\varepsilon_{tot}$  by subtracting the thermal strain  $\varepsilon_{th}$ . Knowing the constitutive model for the stress-strain  
5 relationship of concrete at elevated temperatures, i.e. Eq. (7), the stress distribution can be plotted  
6 as explained earlier in this paper.

7 The equivalent rectangular stress-block can be obtained by considering the equilibrium in forces  
8 and moments between the equivalent block and the actual stress distribution. The stress-block  
9 parameters  $\alpha_{1T}$  and  $\beta_{1T}$  of beam B4 after 1 hr fire exposure were found to be 0.87 and 0.80,  
10 respectively.

11 Fig. 10 indicates that the nonlinear effect of the bottom surface heating is limited to the bottom  
12 zone of the beam cross-section where the tensile reinforcement is allocated while temperature  
13 distribution is uniform in the concrete compression zone. This uniform temperature has  
14 consequently resulted in a linear mechanical strain distribution, because of the constant thermal  
15 strain  $\varepsilon_{th}$ , at the top of the concrete section. The uniform temperature has also resulted in a  
16 constant concrete stress-strain relationship for concrete at different locations in the compression  
17 zone. This explains why the stress distributions at elevated temperatures for beams subjected to  
18 sagging moments have similar shape to the ambient temperature. The uniform average  
19 temperatures in the compression zone were found to be functions of the section width and  
20 aggregate type. Fig. 11 allow predicting the average temperature (based on the average strength)  
21 in the concrete compression zone for both siliceous and carbonate aggregate. Fig. 12 shows the  
22 algebraic average temperature in the concrete compression zone for different aggregate types.

23

## 1 **Stress-block parameters for beams subjected to sagging moments**

2 Tables 3 and 4 show the results of the parametric study for the beams described in Table 1. The  
3 effect of reinforcement ratio and section height on  $\alpha_{1T}$  and  $\beta_{1T}$  is negligible as shown Fig. 13.  
4 The effect of the concrete compressive strength  $f'_c$ , distribution of reinforcing bars, and aggregate  
5 type on the shape of the equivalent stress-block is negligible. On the other hand, the effect of  
6 section width  $b$  is found to have the greatest influence on the studied stress-block parameters  $\alpha_{1T}$   
7 and  $\beta_{1T}$ . This conclusion is reasonable since the effect of the fire temperature is usually limited to  
8 the outer concrete layers exposed to the flames while the beam core remains mostly undamaged.  
9 A statistical study was conducted on the results presented in Tables 3 and 4 to propose a  
10 simplified expression for  $\alpha_{1T}$  and  $\beta_{1T}$ . The effects of fire duration  $t$ , concrete compressive  
11 strength  $f'_c$ , and section width  $b$  were accounted for in a multiple regression analysis using the  
12 Ordinary Least Square method (OLS). Based on the results of the parametric study, Equations  
13 (15.a) and (15.b) were proposed and plotted in Fig. 13. A good matching can be found for all the  
14 results up to 2.50 hr fire duration.

$$15 \quad \alpha_{1T} = \alpha_1 - 1.533 \times 10^{-2} + 24.397 \times 10^{-3} \tau_f + 15.758 \times 10^{-4} f'_c - 10.089 \times 10^{-5} b \quad (15.a)$$

$$16 \quad \beta_{1T} = \beta_1 - 2.907 \times 10^{-2} + 20.734 \times 10^{-3} \tau_f^2 - 94.794 \times 10^{-3} \tau_f - 75.057 \times 10^{-5} f'_c \\ + 15.413 \times 10^{-5} b \quad (15.b)$$

17

## 18 **Flexural capacity for beams subjected to sagging moments**

19 This section presents a methodology that can be used by designers to predict the reduced nominal  
20 flexural resistance  $M_{nT}$  for beams subjected to positive moments under ASTM-E119 standard fire  
21 exposure. This procedure is illustrated considering a 350×750 mm [13.8×29.5 in] rectangular  
22 beam (B30), Fig. 14, cast with a 35 MPa [5076 psi] siliceous aggregate concrete. The beam has

1 reinforcement ratio  $\rho$  (grade 400) is 1.5%. The sectional analysis methodology predicted a  
2 reduced resistance moment after 1.5 hr ASTM-E119 fire exposure of 541 kN.m [ $3.99 \times 10^{11}$  ft.Ib].  
3 The designer can predict the reduced resistance using the proposed equation, Eq. (15), as  
4 explained in Appendix I. Eq. (15) estimates a nominal failure moment of 536 kN.m [ $3.95 \times 10^{11}$   
5 ft.Ib] with a difference of 1% from the sectional analysis. The ASCE simplified method<sup>1</sup>  
6 estimates 496 kN.m [ $3.66 \times 10^{11}$  ft.Ib] (difference is 8% from the sectional analysis methodology).  
7 Applying the 500 °C [932 °F] isotherm method as described in the ENV 1992-1-2<sup>13</sup> requires  
8 constructing the elevated temperatures contour map within the beam cross section, Fig. 15. The  
9 next step is to neglect the concrete where the temperature is above 500 °C [932 °F] in calculating  
10 the reduced flexural strength. As shown in Fig. 15, the reduced cross section is 289×750 mm  
11 [11.4×29.5 in]. Considering this reduced cross section results in 487 kN.m [ $3.59 \times 10^{11}$  ft.Ib]  
12 nominal failure moment, Appendix I. The difference between the 500 °C [932 °F] isotherm  
13 method and the sectional analysis methodology is 10%.

14

### 15 **Calculation of stress-block parameters for beams subjected to Hogging moments**

16 The same procedure illustrated for beams subjected to sagging moments is repeated here. A heat  
17 transfer analysis followed by a sectional analysis was conducted for beam B18 as an illustrative  
18 example. The mechanical strain  $\varepsilon_{cT}$  was isolated from the total strain  $\varepsilon_{tot}$  by subtracting the  
19 thermal strain  $\varepsilon_{th}$ , Fig. 16. Knowing the constitutive model for the stress-strain relationship of  
20 concrete at elevated temperatures, the stress distribution can be predicted at different fire  
21 durations as shown in Fig. 16. The effect of fire on the concrete compression zone becomes more  
22 pronounced in case of negative moments. This effect is characterized by the significant reduction  
23 in the concrete compressive strength and the shape of the compression stress distribution. Fig. 10

1 shows a steep variation in the average temperature in the concrete compression zone allocated  
2 close to the heat source. This variation results in different stress-strain relationships for concrete  
3 at different heights in the compression zone, similar stress distribution was recommended by Tan  
4 and Yao<sup>14</sup>. Therefore, the stress-distribution after 1.0 hr fire exposure has two different peak  
5 points. Tan and Yao have suggested values for  $\alpha_{1T}$  and  $\beta_{1T}$  by replacing  $f'_c$  with  $f'_{cT}$  in Eq. (13)  
6 without having a rational basis for this modification.  $f'_c$  in Eq. (13) is accounting for the  
7 compressive strength enhancement for high strength concrete rather than material weakening at  
8 the top concrete allocated close to fire flames.

9 It should also be noted that concrete failure, i.e. Eq. (8), does have to occur at the top  
10 compression fibers where the maximum mechanical strain occurs. The top concrete fibers should  
11 sustain higher transient strains  $\varepsilon_{tr}$  because of the higher elevated temperatures they experience  
12 which subsequently increase the failure strain  $\varepsilon_{cut}$  predicted by Eq. (10). The equivalent stress-  
13 block can be obtained by considering the equilibrium in forces and moments between the  
14 equivalent block and the actual stress distribution at different fire durations.

15

### 16 **Stress-block parameters for beams subjected to hogging moments**

17 Tables 5 and 6 show the results of the parametric study for the beams presented in Table 2. The  
18 force equilibrium factor  $\alpha_{1T}$  is found to be better described in terms of the fire duration  $\tau_f$  only,  
19 Fig. 17. The moment equilibrium factor  $\beta_{1T}$  is described in terms of the fire duration  $\tau_f$ ,  
20 reinforcement ratio  $\rho$ , aggregate type, concrete compressive strength  $f'_c$ , and section width  $b$ .  
21 Fig. 18 is presented as a sample figure for the results. For simplicity and practicality, the

1 reduction in the concrete compressive strength  $R$  was accounted for in the parameters  $\alpha_{1T}$  and  
2  $\beta_{1T}$  for beams subjected to negative moments.

3 A statistical study was conducted on the results presented in Tables 5 and 6 to propose a  
4 simplified expression for  $\alpha_{1T}$  and  $\beta_{1T}$  for beams subjected to hogging moments. Eq. (16.a) and  
5 (16.b) were proposed based a multiple regression analysis using the Ordinary Least Square (OLS)  
6 method plotted in Figs 17 and 18. A good matching can be found for all the results up to 2.50 hr  
7 fire duration.

$$8 \quad \alpha_{1T} = \alpha_1 - 2.735 \times 10^{-2} - 1.497 \times 10^{-1} \tau_f + 7.579 \times 10^{-2} F_{agg}. \quad (16.a)$$

$$9 \quad \beta_{1T} = \beta_1 - 1.965 \times 10^{-1} - 4.054 \times 10^{-2} \left( \frac{\tau_f}{\rho} \right)^2 + 2.448 \times 10^{-1} \left( \frac{\tau_f}{\rho} \right) - 3.456 \times 10^{-2} F_{agg}. \quad (16.b)$$
$$+ 3.687 \times 10^{-3} f'_c + 2.342 \times 10^{-4} b$$

10 where  $F_{agg}$  is a factor to account for the aggregate type; 0.0 for siliceous concrete and 1.0 for  
11 carbonate concrete.

12

### 13 **Flexural capacity for beams subjected to hogging moments**

14 This section presents a methodology that can be used by designer to predict the flexural resistance  
15  $M_{nT}$  for beam B30 in case of negative bending. The sectional analysis methodology predicted a  
16 reduced resistance moment, after 1.5 hr ASTM-E119 fire exposure, of 627 kN.m [ $4.62 \times 10^{11}$   
17 ft.Ib]. On the other hand, structural engineers can predict a reduced flexural resistance of 593  
18 kN.m [ $4.37 \times 10^{11}$  ft.Ib] using Eq. (16), Appendix II. The ASCE manual<sup>1</sup> recommends using a  
19 reasonable average value for the compressive strength. The 500 °C [932 °F] isotherm method  
20 recommended by the ENV EC2, 1992<sup>13</sup> results in 571 kN.m [ $4.21 \times 10^{11}$  ft.Ib] failure moment  
21 with 9% difference than the sectional analysis.

1  
2  
3  
4  
5  
6  
7  
8  
9  
10  
11  
12  
13  
14  
15  
16  
17  
18  
19  
20  
21  
22

## SUMMARY AND CONCLUSIONS

The sectional analysis methodology, introduced by the authors in a previous publication, is extended in the first part of this paper to cover RC beams subjected to fire from three sides. The proposed methodology is found to be a simple yet accurate method to track the behavior of rectangular RC beams at elevated temperatures. In a similar fashion to ambient temperature analysis of RC beams, temperature-dependent stress-block parameters are developed in the second part of this paper to convert the non-linear compression stresses distribution to a linear and constant stress distribution.

A parametric study aiming at investigating the effect of ASTM-E119 fire temperature on the stress distribution is conducted by applying the proposed methodology on a number of unrestrained rectangular beams. The studied parameters are; fire duration ( $\tau_f$ ), geometry of the sections ( $b$  and  $h$ ), reinforcement ratio ( $\rho$ ) and configuration, concrete compressive strength ( $f'_c$ ), and aggregate type. The studied cross-sections were subjected to a standard ASTM-E119 fire durations up to 2.5 hour. For each time step, the total strain and stress distributions were predicted at failure. The actual distributions of compression stresses at different fire durations were approximated to equivalent stress-blocks. The equivalent stress-block parameters were evaluated for the studied sagging and hogging moment cases by applying a multiple regression analysis on the parametric study results. Failure of beams subjected to sagging moments was found to occur at top compression fibers similar to ambient temperature. On the other hand, failure of beams subjected to hogging moments occurs at a location within the compression block where the mechanical strain in concrete reaches the failure strain at this location. Simplified

1 expressions for the proposed stress-block parameters were derived and verified in this paper for  
2 nominal failure moment prediction. The use of the proposed parameters is relatively easy and  
3 practical to be implemented in design codes. Prediction of nominal flexural strength of fire-  
4 damaged concrete beams can also be useful to check the capacity design of beam-column  
5 assemblage in seismic design.

## 6 7 **ACKNOWLEDGMENTS**

8 This research was funded by the Natural Sciences and Engineering Research Council of Canada  
9 (NSERC).

## 10 11 **REFERENCES**

- 12 1. [Lie, T.T., ed., "Structural Fire Protection," ASCE Manuals and Reports on Engineering](#)  
13 [Practice, no. 78, New York, NY, 1992, 241 pp.](#)
- 14 2. [Kodur, V.K.R., and Dwaikat, M., "Performance-based fire safety design of reinforced](#)  
15 [concrete beams," Journal of Fire Protection Engineering, vol. 17, no. 4, 2007, pp. 293-320.](#)
- 16 3. El-Fitiany, S., Youssef, M.A. 2009, "Assessing the flexural and axial behaviour of reinforced  
17 concrete members at elevated temperatures using sectional analysis", *Fire Safety Journal*, vol.  
18 44, no. 5, pp. 691-703.
- 19 4. Lin, T.D., Gustafarro, A.H., and Abrams, M.S., "Fire Endurance of Continuous Reinforced  
20 Concrete Beam", Portland Cement Association, Bulletin RD072.01B, Skokie, 1981.
- 21 5. [Youssef, M.A., and Rahman, M., "Simplified seismic modelling of reinforced concrete](#)  
22 [flexural members," Magazine of Concrete Research, vol. 59, no. 9, 2007, pp. 639-649.](#)
- 23 6. [Youssef, M.A. and Moftah, M., "General stress-strain relationship for concrete at elevated](#)  
24 [temperatures," Engineering Structures, vol. 29, no. 10, 2007, pp. 2618-2634.](#)

- 1 7. Hertz, K.D., "Concrete Strength for Fire Safety Design," Magazine of Concrete Research,  
2 vol. 57, no. 8, 2005, pp. 445-453.
- 3 8. Terro, M.J., "Numerical modeling of the behavior of concrete structures in fire," ACI  
4 Structural Journal, vol. 95, no. 2, 1998, pp. 183-193.
- 5 9. Bratina, S., Saje, and M., Planinc, I., "The effects of different strain contributions on the  
6 response of RC beams in fire," Engineering Structures, vol. 29, no. 3, 2007, pp. 418-430.
- 7 10. Cement Association of Canada, "Concrete design handbook, CAN/CSA A23.3-04," 3rd Ed.,  
8 Ottawa, 2006.
- 9 11. Collins, M.P., Mitchell, D. 1987, "Prestressed Concrete Basics," Canadian Prestress Concrete  
10 Institute, Ottawa, ON, Canada.
- 11 12. Tassios, T.P., Chronopoulos, M.P., "Structural response of RC elements under fire," The  
12 Structural Engineer, vol. 69, no. 15, 1991, pp. 277-281.
- 13 13. Eurocode 2, "Design of Concrete Structures," ENV EC2, 1992.
- 14 14. Tan, K.H., and Yao, Y., "Fire resistance of four-face heated reinforced concrete columns,"  
15 Journal of Structural Engineering, vol. 129, no. 9, 2003, pp. 1220-1229.
- 16 15. Anderberg, Y, and Thelandersson, S., "Stress and deformation characteristics of concrete at  
17 high temperatures: 2 experimental investigation and material behaviour model", Bulletin 54,  
18 Lund institute of Technology, Sweden, 1976.
- 19 16. Youssef, M.A., El-Fitiany, S.F., and Elfeki, M.A., "Flexural Behavior of Protected Concrete  
20 Slabs After Fire Exposure," Designing Concrete Structures for Fire Safety, ACI SP-255-4,  
21 2008, pp. 47-74.

22  
23  
24

1

**Table 1–Parametric study cases (sagging moment)**

Beam #	$f_y$ (MPa) [psi]	$f_c$ (MPa) [psi]	$b$ (mm) [in]	$h$ (mm) [in]	$\rho$ (% $A_g$ )	Studied variables	Notes
B2				502.5	1.0	$h, \rho$	
B3				[19.8]	2.0	$h, \rho$	
B4			300	705.0	1.0	$h, \rho, b$ , agg. type	
B5			[11.8]	[27.8]	2.0	$h, \rho, b$ , agg. type	
B6		30		907.5	1.0	$h, \rho$	
B7		[4351]		[35.7]	2.0	$h, \rho$	
B8			400	700.0	1.0	$f_c, b$	
B9	400		[15.7]	[27.6]	2.0	$f_c, b$	
B10	[58015]		300	705.0	1.0	aggregate type	carbonate aggregate
B11			[11.8]	[27.8]	2.0	aggregate type	carbonate aggregate
B12				907.5	1.0		
B13			300	[35.7]	2.0		
B14		40	[11.8]	705.0	1.0	RFT configuration	
B15		[5802]		[27.8]	1.0	RFT configuration	2 layers RFT
B16			400	700.0	1.0	$f_c$	
B17			[15.7]	[27.6]	2.0	$f_c$	

2

3

**Table 2–Parametric study cases (hogging moment)**

Beam #	$f_y$ (MPa)	$f_c$ (MPa)	$b$ (mm)	$h$ (mm)	$\rho$ (% $A_g$ )	Studied variables	notes
B18				705.0	1.0	$h, b, \rho$ , agg. type	
B19				[27.8]	2.0	$h, b, \rho$ , agg. type	
B20			300	907.5	1.0	$h, b, \rho$	
B21			[11.8]	[35.7]	2.0	$h, b, \rho$	
B22		30		705.0	1.0	aggregate type	carbonate aggregate
B23		[4351]		[27.8]	2.0	aggregate type	carbonate aggregate
B24	400			700.0	1.0	$b, f_c$	
B25	[58015]			[27.6]	2.0	$b, f_c$	
B26			400	900.0	1.0	$b$	
B27			[15.7]	[35.4]	2.0	$b$	
B28		40		700.0	1.0	$f_c$	
B29		[5802]		[27.6]	2.0	$f_c$	

4

1

**Table 3–Parametric study results (sagging moment)**

$\tau_f$ (hr)	B2		B3		B4		B5		B6		B7		B8		B9	
	$\alpha_{IT}$	$\beta_{IT}$														
0.00	0.846	0.881	0.847	0.880	0.842	0.881	0.845	0.879	0.836	0.886	0.829	0.891	0.834	0.888	0.837	0.885
0.25	0.856	0.852	0.855	0.852	0.847	0.856	0.850	0.860	0.846	0.857	0.844	0.858	0.839	0.869	0.842	0.865
0.50	0.860	0.828	0.863	0.825	0.860	0.830	0.850	0.830	0.854	0.831	0.851	0.833	0.843	0.846	0.847	0.844
0.75	0.861	0.817	0.866	0.813	0.860	0.816	0.861	0.815	0.857	0.818	0.858	0.817	0.850	0.832	0.851	0.831
1.00	0.870	0.803	0.874	0.800	0.870	0.802	0.872	0.800	0.870	0.802	0.873	0.799	0.850	0.826	0.858	0.820
1.25	0.879	0.796	0.882	0.790	0.879	0.793	0.880	0.790	0.877	0.792	0.878	0.791	0.857	0.817	0.862	0.811
1.50	0.880	0.789	0.886	0.782	0.882	0.786	0.885	0.782	0.883	0.784	0.884	0.782	0.862	0.809	0.868	0.803
1.75	0.885	0.782	0.887	0.778	0.885	0.779	0.887	0.777	0.886	0.778	0.888	0.776	0.867	0.803	0.873	0.796
2.00	0.891	0.778	0.891	0.772	0.887	0.775	0.890	0.772	0.888	0.774	0.890	0.771	0.870	0.799	0.878	0.792
2.25	0.887	0.775	0.891	0.769	0.890	0.772	0.892	0.768	0.889	0.771	0.892	0.768	0.876	0.793	0.880	0.787
2.50	0.887	0.772	0.892	0.766	0.890	0.768	0.892	0.765	0.892	0.767	-----	-----	0.882	0.791	-----	-----

2

3

**Table 4–Parametric study results (sagging moment) - Cont'd**

$\tau_f$ (hr)	B2		B3		B4		B5		B6		B7		B8		B9	
	$\alpha_{IT}$	$\beta_{IT}$														
0.00	0.844	0.881	0.845	0.879	0.802	0.902	0.806	0.899	0.810	0.898	0.811	0.897	0.801	0.906	0.802	0.902
0.25	0.846	0.860	0.845	0.861	0.819	0.869	0.817	0.871	0.824	0.868	0.823	0.868	0.811	0.882	0.809	0.882
0.50	0.854	0.834	0.858	0.831	0.831	0.841	0.837	0.837	0.833	0.842	0.834	0.840	0.822	0.859	0.826	0.853
0.75	0.858	0.822	0.859	0.820	0.839	0.826	0.840	0.825	0.838	0.828	0.839	0.826	0.824	0.845	0.830	0.840
1.00	0.869	0.806	0.871	0.804	0.854	0.810	0.854	0.810	0.854	0.813	0.854	0.810	0.826	0.837	0.833	0.832
1.25	0.877	0.796	0.879	0.793	0.863	0.800	0.869	0.794	0.862	0.801	0.866	0.797	0.836	0.830	0.841	0.823
1.50	0.883	0.787	0.885	0.785	0.870	0.791	0.875	0.786	0.869	0.792	0.873	0.790	0.839	0.822	0.852	0.811
1.75	0.888	0.781	0.889	0.779	0.876	0.783	0.881	0.779	0.874	0.786	0.878	0.782	0.845	0.817	0.856	0.806
2.00	0.889	0.777	0.892	0.773	0.879	0.779	0.883	0.775	0.881	0.782	0.881	0.778	0.855	0.811	0.862	0.799
2.25	0.892	0.772	0.893	0.769	0.883	0.775	0.886	0.771	0.881	0.777	0.886	0.773	0.859	0.803	0.866	0.795
2.50	0.895	0.769	0.895	0.765	0.885	0.771	0.888	0.767	0.881	0.775	0.887	0.768	0.856	0.804	0.868	0.792

1

**Table 5–Parametric study results (hogging moment)**

$\tau_f$ (hr)	B2		B3		B4		B5		B6		B7	
	$\alpha_{IT}$	$\beta_{IT}$										
0.00	0.843	0.845	0.835	0.829	0.842	0.845	0.834	0.837	0.833	0.832	0.797	0.801
0.25	0.805	0.820	0.813	0.817	0.838	0.839	0.798	0.818	0.800	0.815	----	0.773
0.50	0.696	0.755	0.722	0.765	----	0.788	----	0.752	0.685	0.736	----	----
0.75	0.631	0.705	0.659	0.719	0.743	0.758	0.638	0.691	0.663	0.694	----	----
1.00	0.557	0.660	0.598	0.691	0.707	0.761	0.572	0.662	0.613	0.653	0.518	0.605
1.25	0.491	0.604	0.536	0.640	0.668	0.739	0.515	0.627	0.559	0.615		0.575
1.50	0.439	0.553	0.483	0.593	0.631	0.717	0.464	0.585	0.510	0.573	0.410	0.530
1.75	0.396	0.508	0.437	0.548	0.596	0.693	0.422	0.543	0.468	0.532	0.371	0.492
2.00	0.359	0.468	0.399	0.507	0.564	0.667	0.387	0.505	0.431	0.495	----	0.452
2.25	0.327	0.432	0.366	0.471	0.534	0.641	0.357	0.473	0.399	0.462	0.310	0.423
2.50	0.298	0.400	0.336	0.438	0.507	0.616	0.330	0.442	0.371	0.433	0.285	----

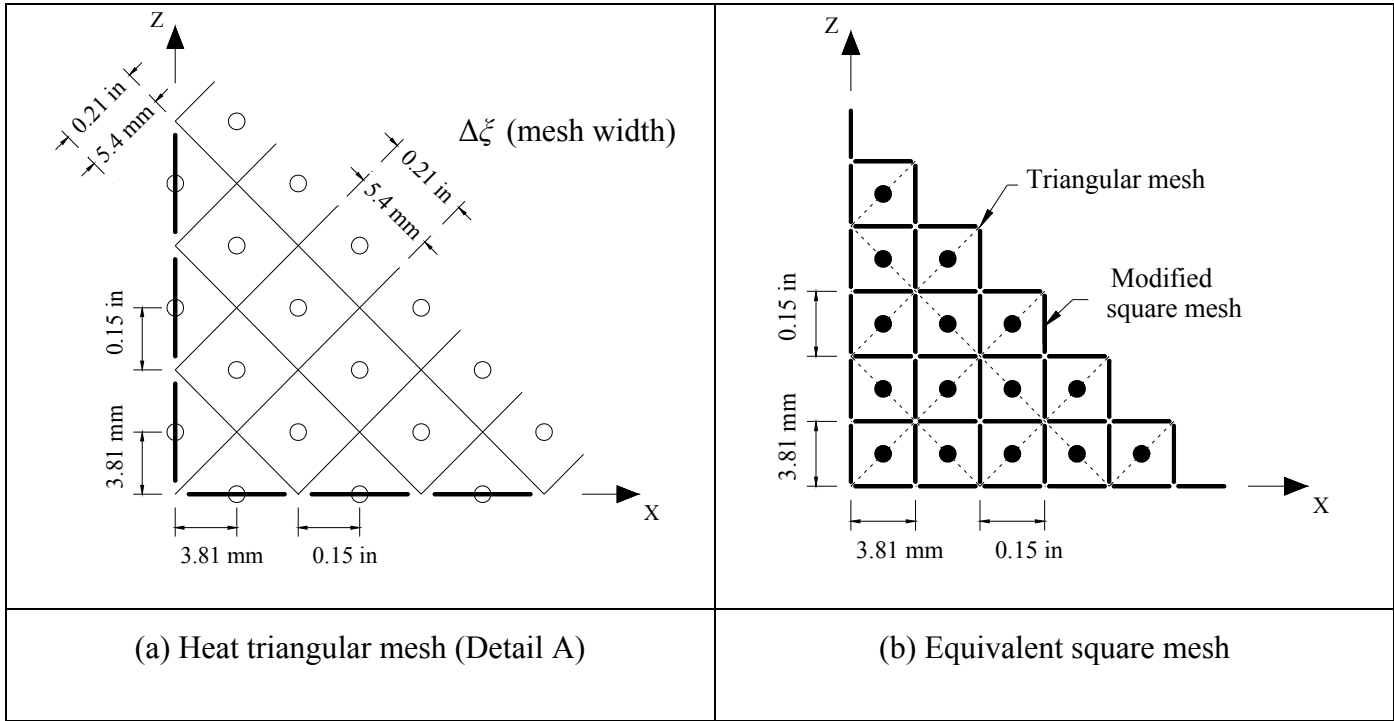
2

3

**Table 6–Parametric study results (hogging moment) - Cont'd**

$\tau_f$ (hr)	B2		B3		B4		B5		B6		B7	
	$\alpha_{IT}$	$\beta_{IT}$										
0.00	0.881	0.879	0.886	0.891	0.881	0.879	0.888	0.885	0.887	0.887	0.906	0.902
0.25	0.927	0.902	0.915	0.898	0.912	0.892	0.933	0.908	0.925	0.909	----	0.930
0.50	0.995	0.933	0.968	0.919	----	0.918	----	0.944	0.994	0.953	----	----
0.75	1.047	0.964	1.012	0.944	0.989	0.937	1.055	0.982	1.021	0.982	----	----
1.00	1.101	0.993	1.057	0.961	1.022	0.945	1.110	1.005	1.063	1.013	1.167	1.050
1.25	1.140	1.021	1.091	0.984	1.057	0.964	1.157	1.033	1.106	1.043	----	1.081
1.50	1.173	1.045	1.123	1.002	1.089	0.985	1.191	1.063	1.142	1.074	1.250	1.115
1.75	1.200	1.068	1.150	1.022	1.114	1.007	1.223	1.087	1.170	1.098	1.276	1.140
2.00	1.221	1.089	1.173	1.042	1.130	1.028	1.246	1.110	1.196	1.121	----	1.166
2.25	1.240	1.108	1.193	1.059	1.140	1.047	1.268	1.131	1.218	1.143	1.318	1.187
2.50	1.255	1.126	1.209	1.075	1.150	1.060	1.287	1.152	1.239	1.163	1.333	----



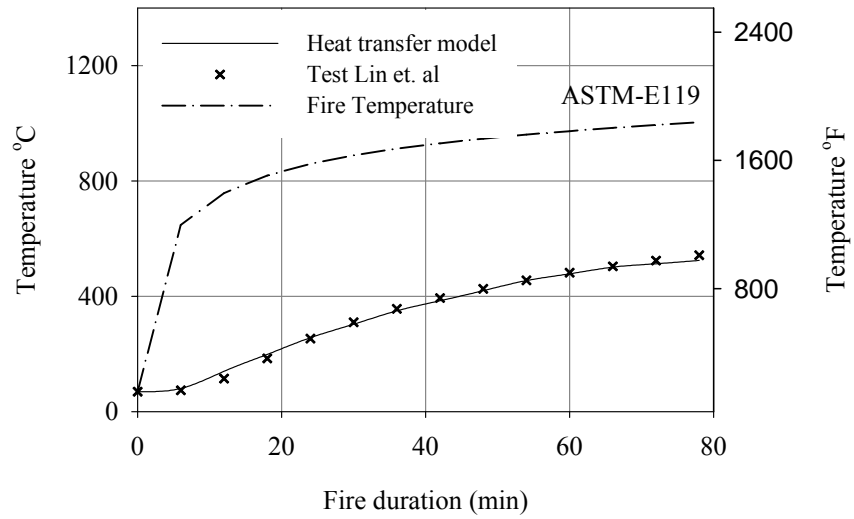


1

**Fig. 2-Heat Transfer mesh of beam B1**

2

3



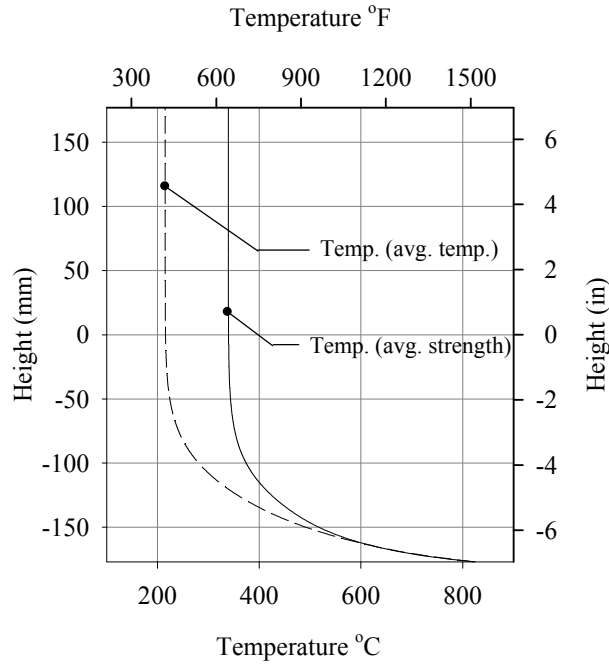
4

5

6

7

**Fig. 3. Validation of the heat transfer model (average temperature of bottom reinforcing bars)**



1

2 **Fig. 4-Average temperature distributions for B1 after 1hr ASTM-E119 fire exposure**

3

4

5

6

7

8

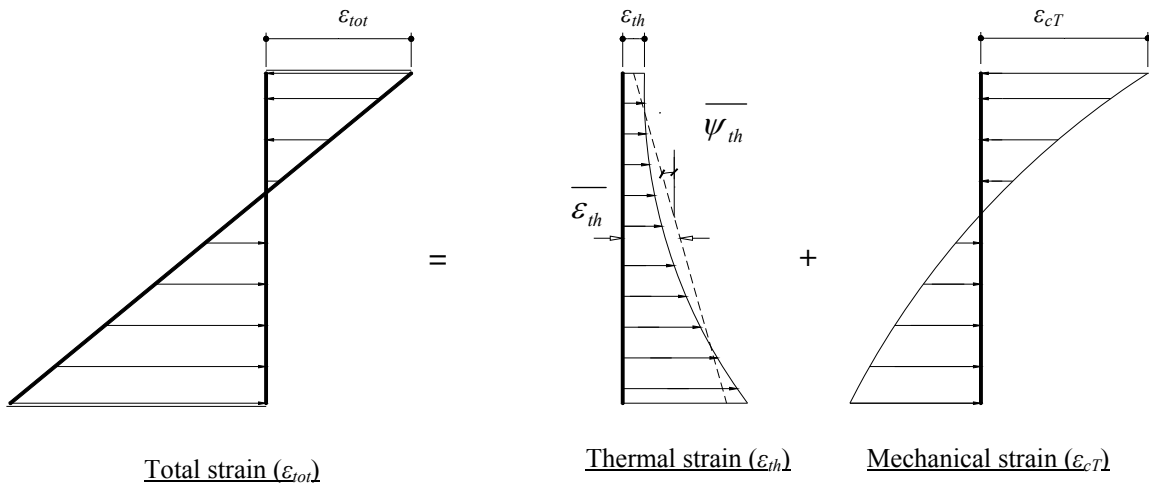
9

10

11

12

13



14

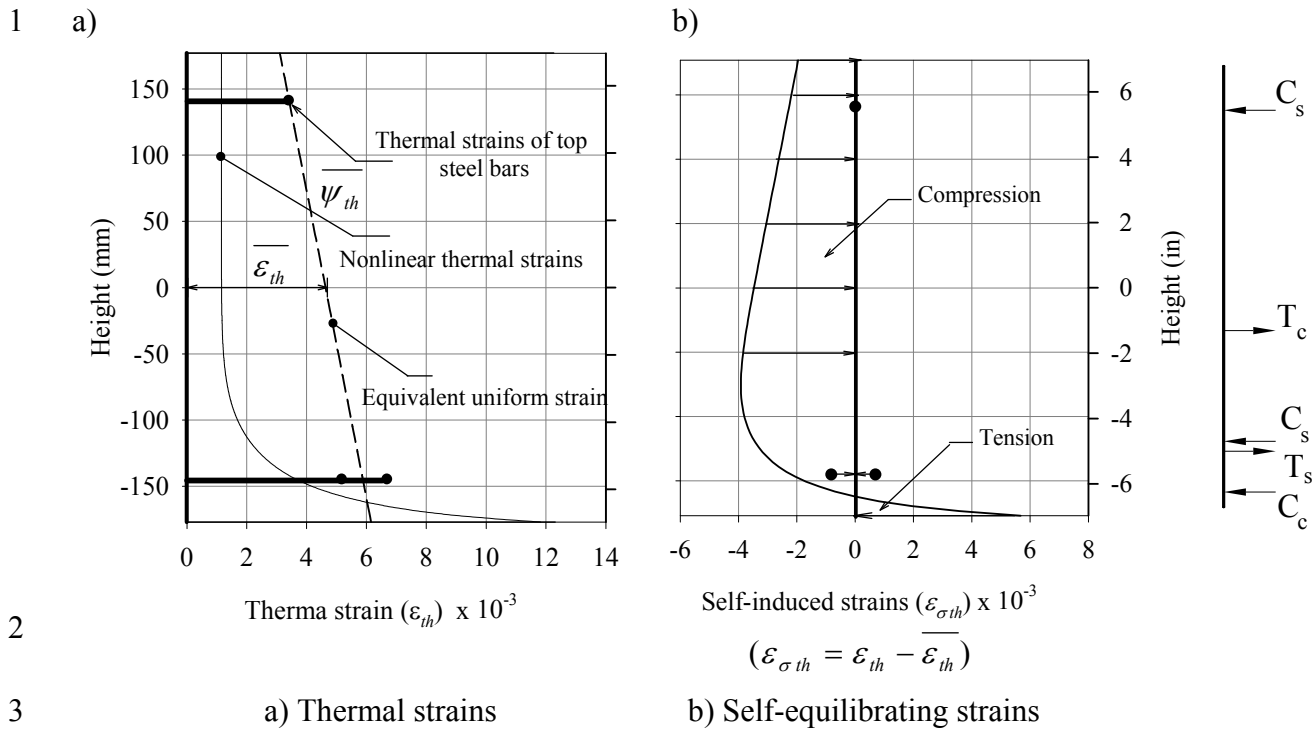
**Fig. 5-Components of total strain at elevated temperatures**

15

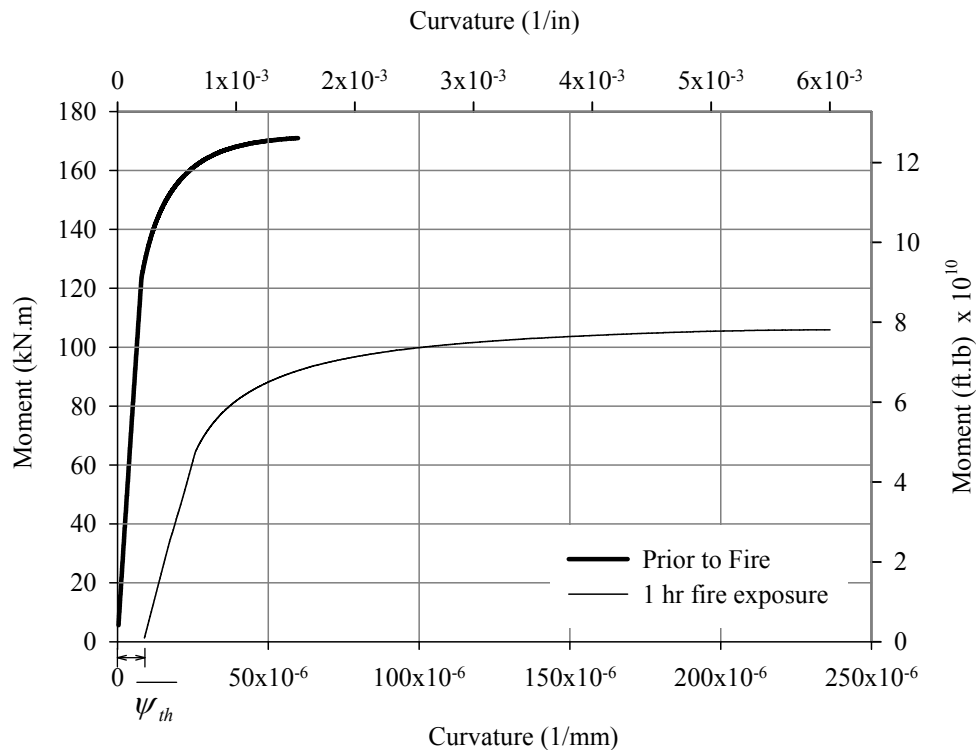
16

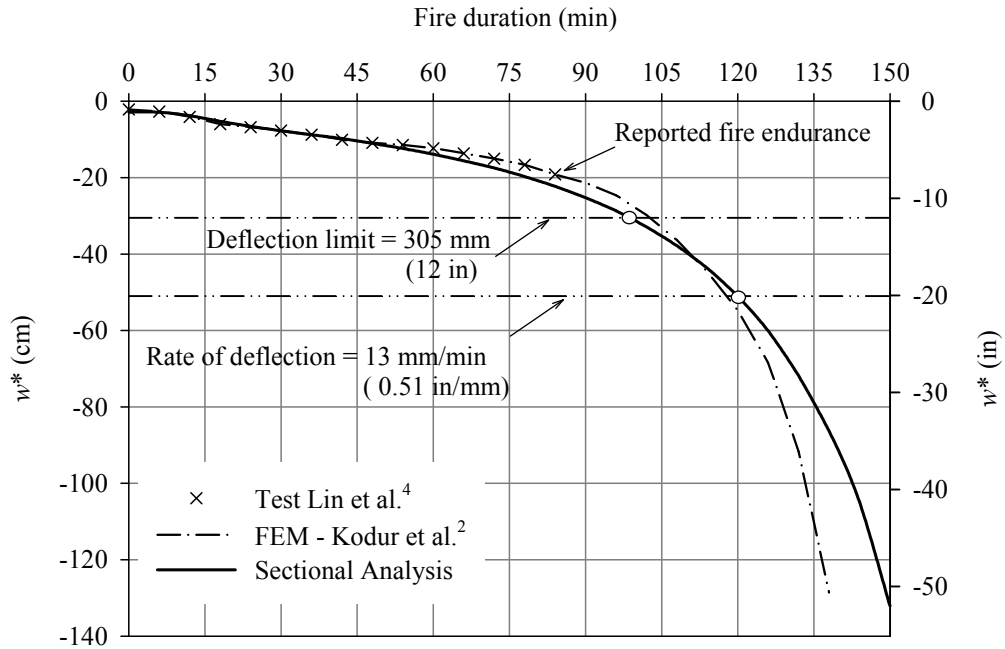
17

18

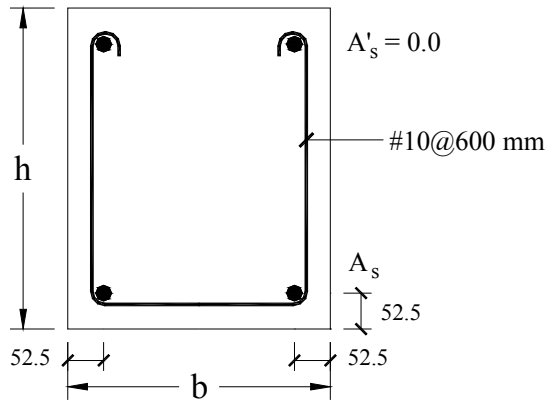


4 **Fig. 6-Strain distribution and self-equilibrating forces along B1 height**



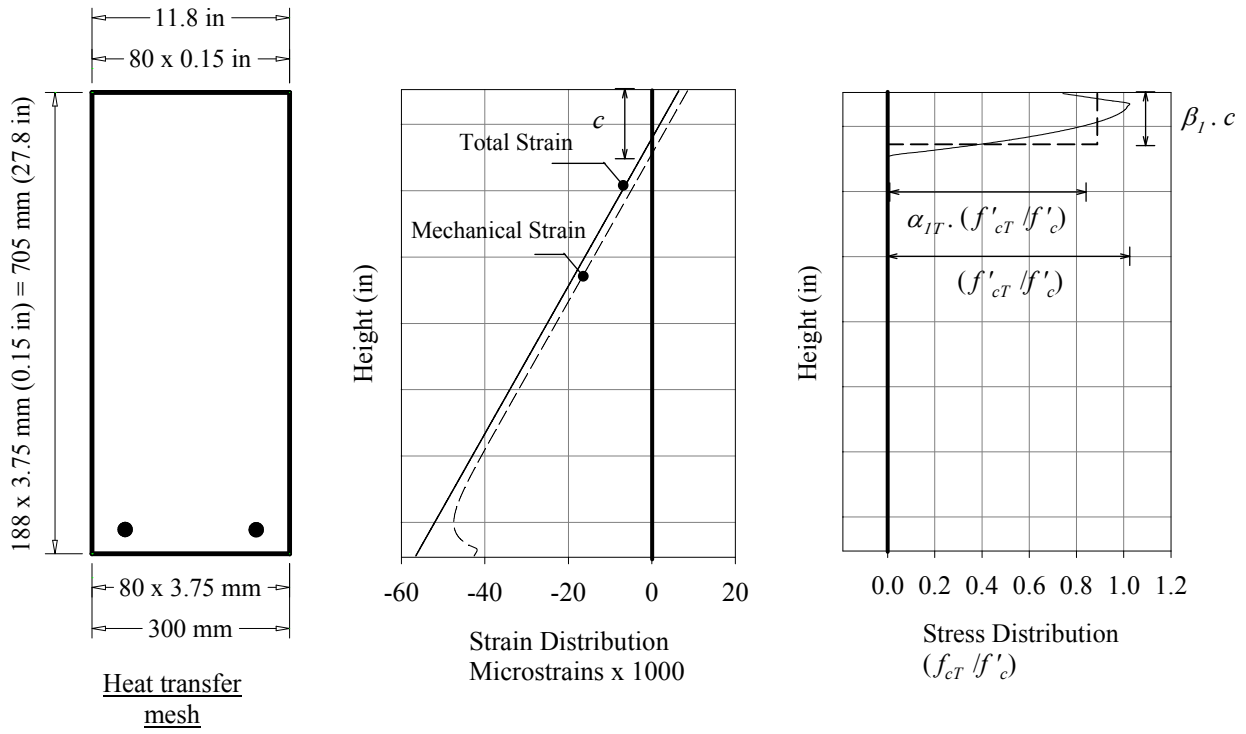


1  
2 **Fig. 8-Validation of sectional analysis methodology by prediction the deflections of B1**  
3 **during fire exposure**



4  
5  
6  
7  
8  
9  
10 **Fig. 9-Details of the studied RC beam "B4" in the parametric study**  
11 **Dimensions in mm [1 in = 25.4 mm]**

1  
2  
3  
4  
5  
6  
7  
8  
9



10  
11  
12

**Fig. 10-Strain and stress distributions of B4 at 1.0 hr fire exposure**

13  
14  
15

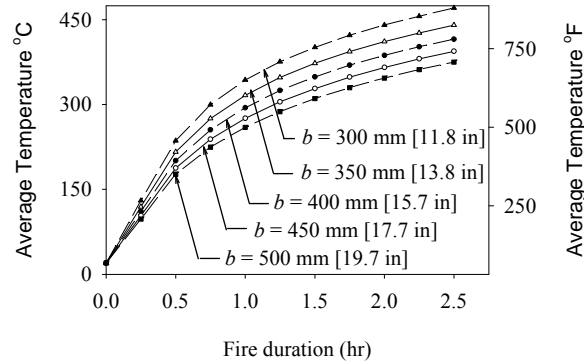
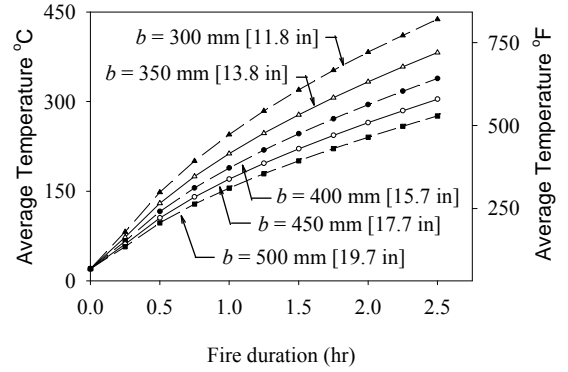
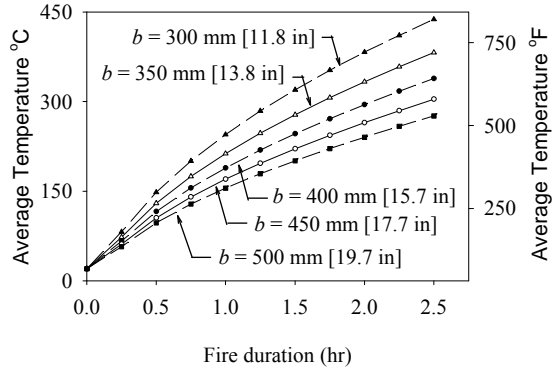


**Fig. 11-Effect of ASTM-E119 fire duration and section width on the average strength temperatures**



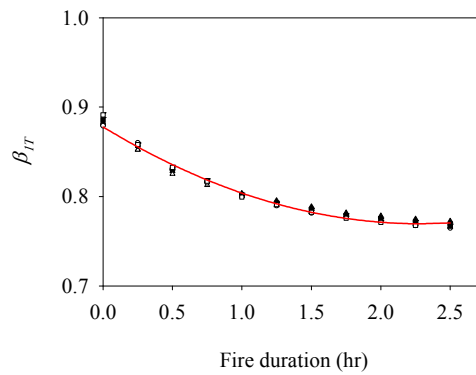
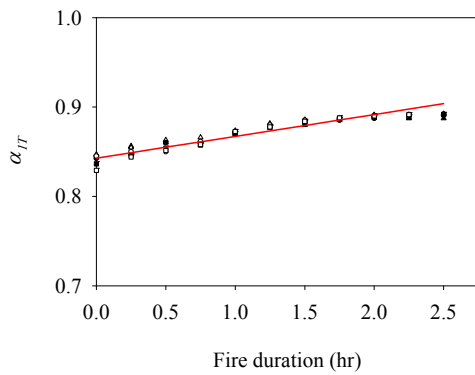
1  
2  
3

a) Siliceous aggregate

b) Carbonate aggregate

**Fig. 12-Effect of ASTM-E119 fire duration and section width on the average temperature**

4  
5  
6  
7



B2 (300 x 503, r = 1%)  
B3 (300 x 503, r = 2%)  
B4 (300 x 705, r = 1%)  
B5 (300 x 705, r = 2%)  
B6 (300 x 908, r = 1%)  
B7 (300 x 908, r = 2%)  
Eq. (15)

8  
9  
10

a) Variation of  $\alpha_{1T}$

b) Variation of  $\beta_{1T}$

**Fig. 13-Effect of fire duration, RFT ratio, and section height on  $\alpha_{1T}$  and  $\beta_{1T}$**

Dimensions in mm [1 in = 25.4 mm]

11  
12  
13  
14  
15  
16  
17  
18  
19  
20  
21  
22

1  
2  
3  
4  
5  
6  
7  
8  
9  
10  
11  
12  
13  
14  
15  
16  
17  
18  
19  
20  
21  
22  
23  
24  
25  
26  
27  
28  
29  
30  
31  
32  
33  
34

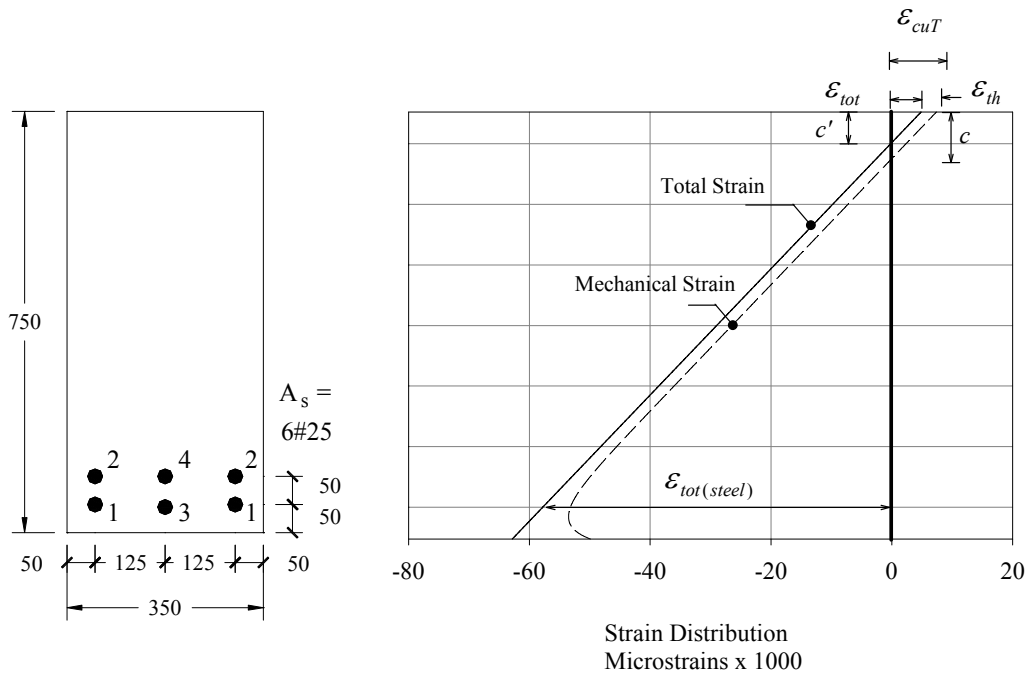


**Fig. 14- Example beam (B30) for calculating the nominal failure moment  $M_{nT}$  using the proposed  $\alpha_{1T}$  and  $\beta_{1T}$  - Dimensions in mm [1 in = 25.4 mm]**

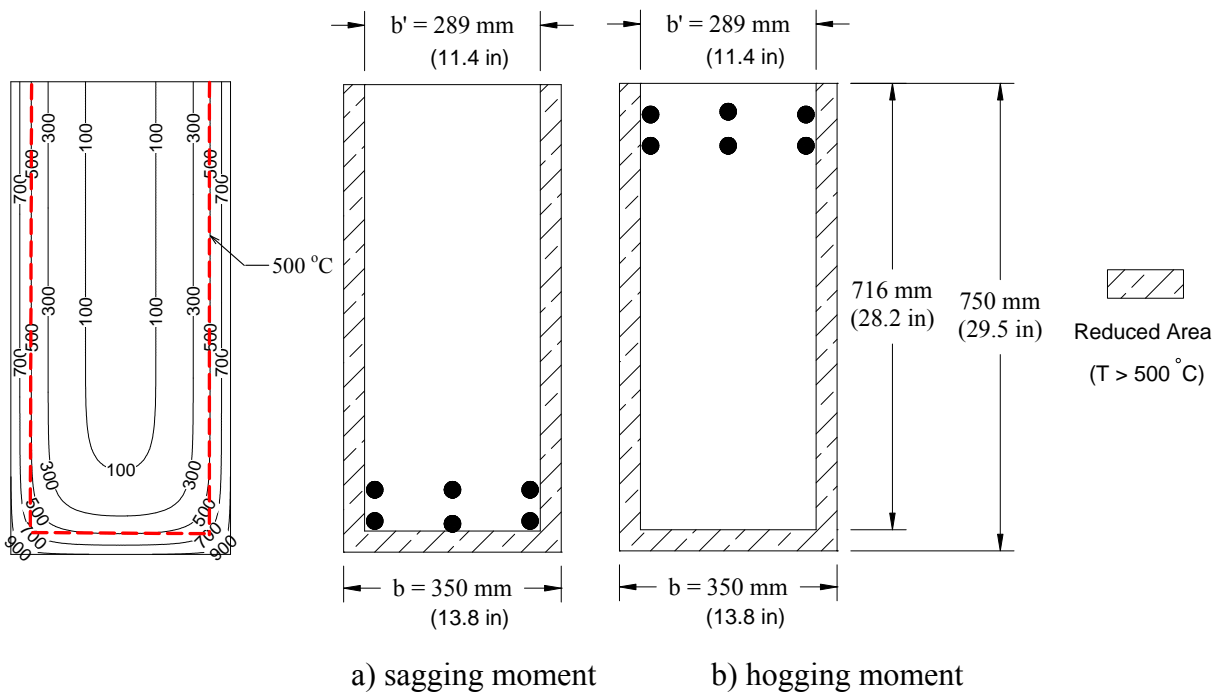


**Fig. 15- Temperature contour map in °C of B30 [1 °F = 1.8 °C + 32]**

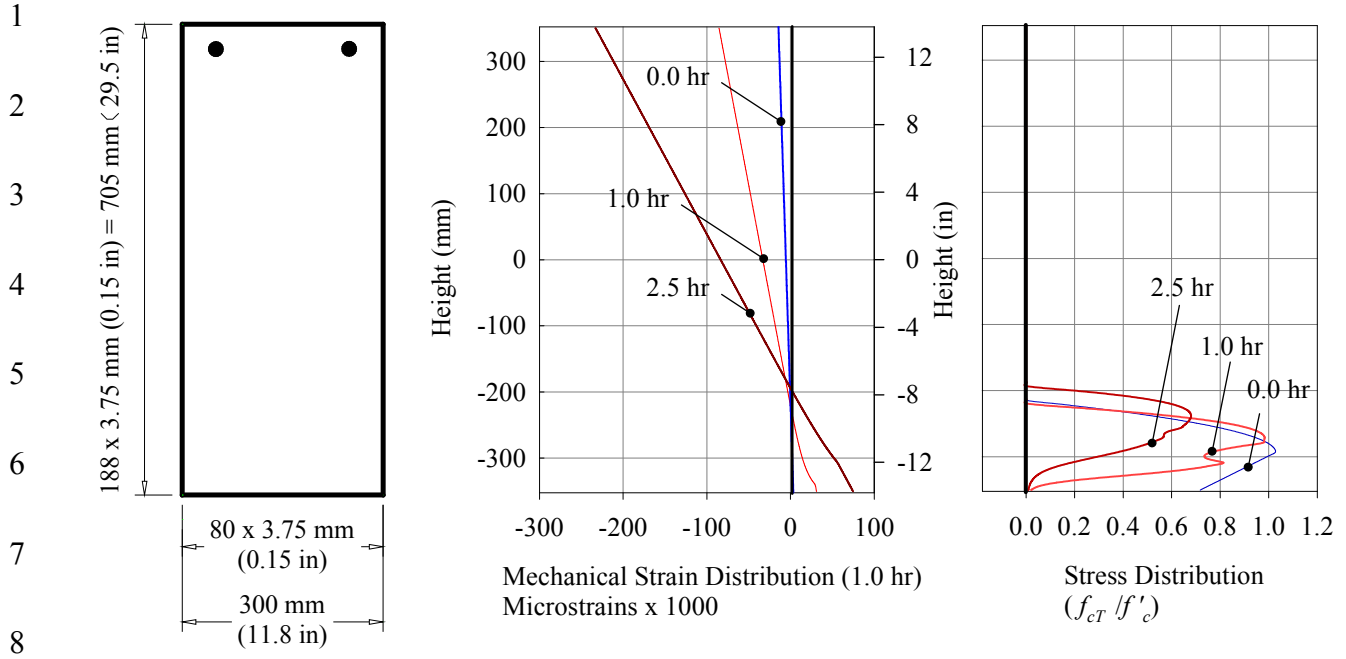


Fig. 16-Mechanical strain and stress distributions of B18 at different fire durations

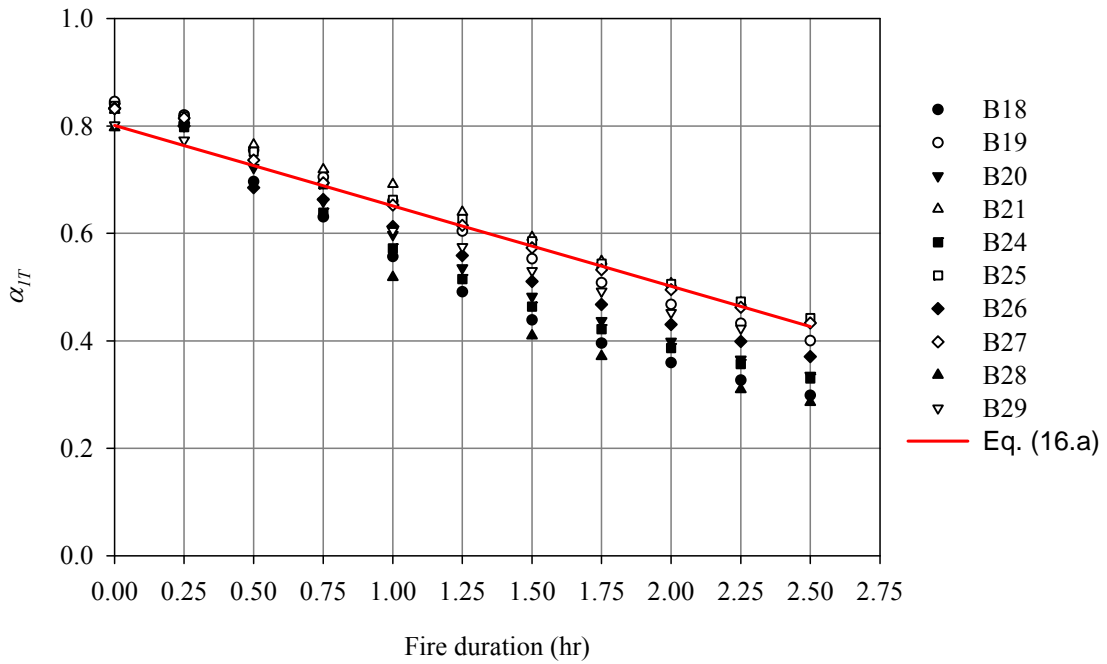
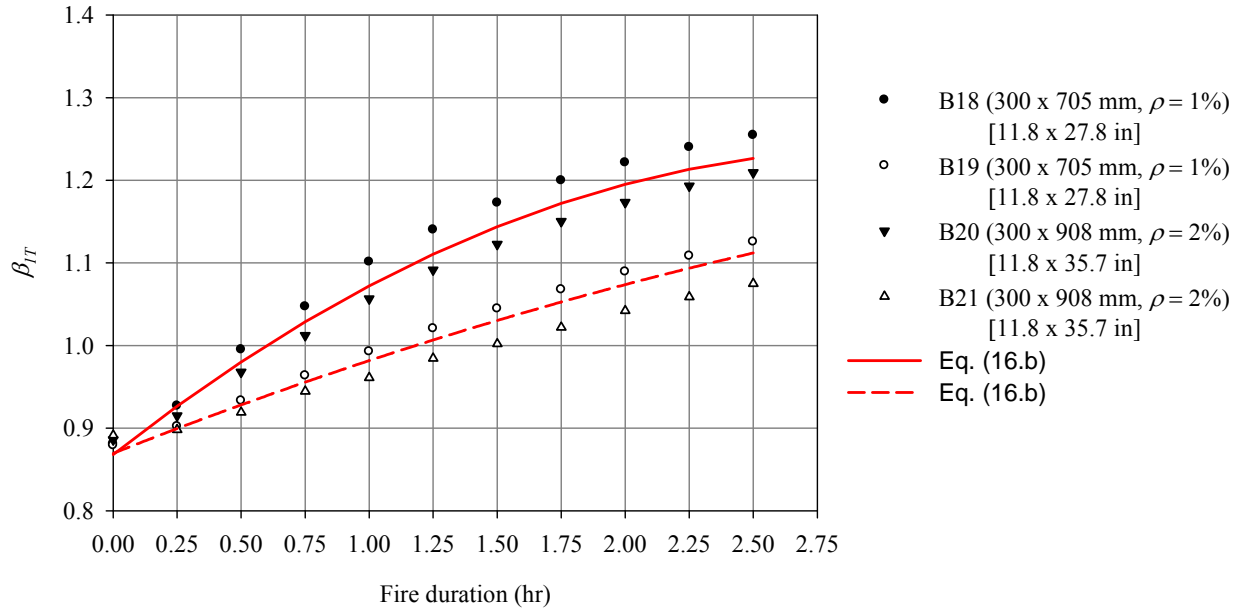


Fig. 17- Effect of fire duration and other studied factors on  $\alpha_{1T}$



1  
2

3

**Fig. 18- Effect of fire duration, RFT ratio, and section height on  $\beta_{TT}$**

4  
5  
6  
7  
8  
9  
10  
11  
12  
13  
14  
15  
16  
17  
18  
19  
20  
21  
22  
23  
24  
25  
26  
27  
28

## Appendix I

### 2 *Simplified calculation of the $M_{nT}$ for beams subjected to sagging moments*

3 1. The reduced concrete compressive strength can be calculated using **Fig. 15 and Eq. (2.b)**

4 for  $b = 350$  mm [13.8 in] and  $t = 1.50$  hr  $\rightarrow T_{av. str} = 373$  °C [703 °F] [Fig. 15]

5  $R = 1.0$  [Eq. (2.b)]

6  $f'_{cT} = 1.25 \times (1.0 \times f'_c) \leq f'_c$  [25% increase because beam is loaded before fire]

7  $\therefore f'_{cT} = f'_c = 35$  MPa [5076 psi]

8  $f'_{cT} = K_{hT} \times f'_{cT} = 1.0 \times 35$  MPa [neglect confinement]

9 2. The compression force in the concrete is calculated as follows

10  $C = \alpha_{1T} \times f'_{cT} \times \beta_{1T} \times c \times b$  [Eq. (15.a) and (15.b)]

11  $\alpha_1 = 0.85 - 0.0015 \times 35 = 0.80$

12  $\therefore \alpha_{1T} = 0.80 - 1.533 \times 10^{-2} + 24.397 \times 10^{-3} \times 1.50 + 15.758 \times 10^{-4} \times 35 - 10.089 \times 10^{-5} \times 350$   
 $= 0.84$

13  $\beta_1 = 0.97 - 0.0025 \times 35 = 0.88$

14  $\therefore \beta_{1T} = 0.88 - 2.907 \times 10^{-2} + 20.734 \times 10^{-3} \times 1.5^2 - 94.794 \times 10^{-3} \times 1.5 - 75.057 \times 10^{-5} \times 35$   
 $+ 15.413 \times 10^{-5} \times 350 = 0.78$

15  $C = 0.83 \times 35 \times 0.79 \times c \times 350 = 8,026.2 \times c$

16 assume  $c = 105.9$  mm [4.2 in]  $\rightarrow \therefore C = 849991$  N [191.1 kps]

17 3. The tension force in the steel is calculated as follows

18  $\epsilon_{cuT} = \epsilon_{cu} + \epsilon_{tr}$

19 for  $b = 350$  mm [13.8 in] and  $t = 1.50$  hr  $\rightarrow T_{av. temp} = 278$  °C [532 °F] [Fig. 16.a]

20  $\epsilon_{tr} = 0.00593$  [Eq. (5)]

21  $\epsilon_{cuT} = 0.0035 + 0.00593 = 0.00943$  [Eq. (8)]

1  $\varepsilon_{tot} = \varepsilon_{cuT} - \varepsilon_{th} = 0.00943 - 0.00167 = 0.00776$  [Fig. (22)]

2  $c' = \frac{c}{\varepsilon_{cuT}} \times \varepsilon_{tot} = 0.823 \times c$

3  $\varepsilon_{tot(steel)} = \frac{\varepsilon_{tot}}{c'} \times d$  [Fig. (22)]

4  $T_1 = 558 \text{ }^\circ\text{C}$  [1036 °F],  $T_2 = 420 \text{ }^\circ\text{C}$  [788 °F],  $T_3 = 376 \text{ }^\circ\text{C}$  [709 °F], and  $T_4 = 163 \text{ }^\circ\text{C}$  [325  
5 °F]

6  $\varepsilon_{sT} = \varepsilon_{tot} - \varepsilon_{th}$  [Fig. (22)]

7 The coefficient of thermal expansion of steel  $\alpha_s$  is given by Lie et al. as follows

8  $\alpha_s = (0.004T + 12) \times 10^{-6} \text{ }^\circ\text{C}^{-1}$   $T < 1000 \text{ }^\circ\text{C}$  [1832 °F]

9  $\alpha_s = 16 \times 10^{-6} \text{ }^\circ\text{C}^{-1}$   $T \geq 1000 \text{ }^\circ\text{C}$  [1832 °F]

10 Thus,

11  $\varepsilon_{sT1} = 0.04661$ ,  $\varepsilon_{sT2} = 0.04436$ ,  $\varepsilon_{sT3} = 0.04949$ , and  $\varepsilon_{sT4} = 0.04805$

12  $f_{sT1} = 219 \text{ MPa}$  [31764 psi],  $f_{sT2} = 282 \text{ MPa}$  [40901 psi],  $f_{sT3} = 303 \text{ MPa}$  [43947 psi], and

13  $f_{sT4} = 397 \text{ MPa}$  [57581 psi]

14  $T_s = \sum_{i=1}^4 f_{sTi} \times A_{si} = 849991 \text{ N}$  [191.1 kps]

15  $C = T_s$  O.K.

16  $M_{nT} = \sum_{i=1}^4 f_{sTi} \times A_{si} \times (d_i - \frac{\beta_{1T} \times c}{2}) = 536 \text{ kN.m}$  [39.54 × 10<sup>4</sup> ft.lb]

17  
18

19

20

## Appendix II

### 2 *Simplified calculation of the $M_{nT}$ for beams subjected to hogging moments*

1. The compression force in the concrete is calculated as follows

$$C = \alpha_{1T} \times f'_c \times \beta_{1T} \times c \times b$$

$$\alpha_1 = 0.85 - 0.0015 \times 35 = 0.80$$

$$\alpha_{1T} = \alpha_1 - 2.735 \times 10^{-2} - 1.497 \times 10^{-1} \times 1.50 + 7.579 \times 10^{-2} \times 0.0 = 0.55$$

$$\beta_1 = 0.97 - 0.0025 \times 35 = 0.88$$

$$\begin{aligned} \beta_{1T} = \beta_1 - 1.965 \times 10^{-1} - 4.054 \times 10^{-2} \left( \frac{1.5}{1.5} \right)^2 + 2.448 \times 10^{-1} \left( \frac{1.5}{1.5} \right) - 3.456 \times 10^{-2} \times 0.0 \\ + 3.687 \times 10^{-3} \times 35 + 2.342 \times 10^{-4} \times 350 = 1.10 \end{aligned}$$

assume  $c = 132.9$  mm [5.2 in]

$$\therefore C = 984734 \text{ N [221.4 kps]}$$

2. The tension force in the steel is calculated as follows

$$T_1 = 366 \text{ }^\circ\text{C [691 }^\circ\text{F]}, T_2 = 366 \text{ }^\circ\text{C [691 }^\circ\text{F]}, T_3 = 58 \text{ }^\circ\text{C [136 }^\circ\text{F]}, \text{ and } T_4 = 58 \text{ }^\circ\text{C [136 }^\circ\text{F]}$$

$$f_{yT1} = 296 \text{ MPa [42932 psi]}, f_{yT2} = 296 \text{ MPa [42932 psi]}, f_{yT3} = 393 \text{ MPa [57001 psi]}, \text{ and}$$

$$f_{yT4} = 393 \text{ MPa [57001 psi]}$$

$$T_s = \sum_{i=1}^4 f_{sTi} \times A_{si} = 984734 \text{ N [221.4 kps]}$$

$$C = T_s \quad \text{O.K.}$$

$$M_{nT} = \sum_{i=1}^4 f_{sTi} \times A_{si} \times \left( d_i - \frac{\beta_{1T} \times c}{2} \right) = 593 \text{ kN.m} \quad [43.75 \times 10^4 \text{ ft.lb}] \quad (\text{Diff. } \approx 5\%)$$

18

19

## TABLES AND FIGURES

1

### 2 List of Tables

3 Table 1–Parametric study cases (sagging moment)

4 Table 2–Parametric study cases (hogging moment)

5 Table 3–Parametric study results (sagging moment)

6 Table 4–Parametric study results (sagging moment) - Cont'd

7 Table 5–Parametric study results (hogging moment)

8 Table 6–Parametric study results (hogging moment) - Cont'd

9

### 10 List of Figures

11 Fig. 1-Beam B1 loading and configuration

12 Fig. 2-Heat Transfer mesh of beam B1

13 Fig. 3. Validation of the heat transfer model (average temperature

14 Fig. 4-Average temperature distributions for B1 after 1hr ASTM-E119 fire exposure

15 Fig. 5-Components of total strain at elevated temperatures

16 Fig. 6-Strain distribution and self-equilibrating forces along B1 height

17 Fig. 7-Effect of fire temperature on the moment – curvature relationship for B1

18 **Fig. 8-Validation of sectional analysis methodology by prediction the deflections of B1**  
19 **during fire exposure**

20 Fig. 9-Details of the studied RC beam “B4” in the parametric study

21 Fig. 10-Strain and stress distributions of B4 at 1.0 hr fire exposure

22 Fig. 11-Effect of ASTM-E119 fire duration and section width on the average

23 **Fig. 12-Effect of ASTM-E119 fire duration and section width on the average temperature**

24 Fig. 13-Effect of fire duration, RFT ratio, and section height on  $\alpha_{1T}$  and  $\beta_{1T}$

25 Fig. 14- Example beam (B30) for calculating the nominal failure moment  $M_{nT}$  using the  
26 proposed  $\alpha_{1T}$  and  $\beta_{1T}$  - Dimensions in mm [1 in = 25.4 mm]

27 **Fig. 15- Temperature contour map in °C of B30**

28 Fig. 16-Mechanical strain and stress distributions of B18 at different fire durations

29 **Fig. 17- Effect of fire duration and other studied factors on  $\alpha_{1T}$**

30 **Fig. 18- Effect of fire duration, RFT ratio, and section height on  $\beta_{1T}$**

31

32

33

34

35

36

- 1
- 2
- 3
- 4
- 5
- 6
- 7
- 8
- 9